This is a preprint, the final version is subject to change, of the American Mineralogist (MSA)
Cite as Authors (Year) Title. American Mineralogist, in press.
(DOI will not work until issue is live.) DOI: http://dx.doi.org/10.2138/am.2013.4295

Revision 1

Manuscript submitted to the Special Section: "Mineralogy and the Nuclear Industry: Actinides in Geology, Energy, and the Environment"

Evidence for nanocrystals of vorlanite, a rare uranate mineral, in the Nopal I low-temperature uranium deposit (Sierra Peña Blanca, Mexico)

Guillaume Othmane,[1,*] Thierry Allard,[1] Nicolas Menguy,[1] Guillaume Morin,[1] Imène Esteve,[1] Mostafa Fayek,[2] and Georges Calas[1]

[1] Institut de Minéralogie et de Physique des Milieux Condensés (IMPMC), UMR 7590 CNRS-UPMC/Paris VI-IRD, Case 115, 4 place Jussieu, 75252 Paris Cedex 05, France

[2] Dept. of Geological Sciences, University of Manitoba, Winnipeg, MB, Canada R3T 2N2

* E-mail: Guillaume.Othmane@impmc.upmc.fr

ABSTRACT

The occurence of vorlanite, cubic $CaUO_4$, is reported in the Nopal I uranium deposit (Sierra Peña Blanca, Mexico). This is the first time this rare calcium uranate has been found displaying a cubic morphology, in agreement with its crystal structure. Vorlanite occurs as nanoscale crystals embedded in U-bearing opal, with a Ca/U ratio of ~ 1. Association with opal suggests that vorlanite formed at Nopal during late stage U-mobilization under oxidizing conditions and low (< 50 °C) temperature. The presence of nanoscale uranate crystals in an environment largely dominated by uranyl silicates indicates that uranates may play a role in uranium scavenging at low temperature. In addition, the occurrence of vorlanite in the crystal shape consistent with its structure provides unique information on its conditions of formation.

Keywords: vorlanite, cubic $CaUO_4$, uranate, nanoscale crystal, opal, Nopal

INTRODUCTION

Uranium migration in geological formations has major geochemical, economical and environmental applications (Ragnarsdottir and Charlet 2000). Under oxidizing conditions, soluble hexavalent uranium occurs as uranyl groups complexed by various anions (Langmuir 1978). The fate of uranium in environmental systems is affected by several mechanisms, including precipitation, adsorption onto minerals, amorphous materials or organic matter, and absorption by organisms (e.g., Duff et al. 2002). Colloidal-facilitated transport of actinides may be an additional transport process (Novikov et al. 2006). In silica-saturated waters, uranium trapping mechanisms include adsorption on silica colloids, as shown by Allard et al. (1999) during the oxidative weathering of the Peny (Massif Central, France) uranium deposit, underlining the importance of silicate ligands.

Recently, Schindler et al. (2010) investigated uranium speciation in recent and low temperature opals from the Nopal I uranium deposit (Sierra Peña Blanca, Mexico) (Calas et al. 2008 and references therein; Angiboust et al. 2012). They found that opal was zoned with respect to Ca and U, retaining an almost constant atomic ratio of 1:1, and suggested a mechanism of trapping Ca-U-particles or aqueous species by colloidal silica.

We present new data on the Ca-U species occurring in the opals from Nopal I, in order to constrain the chemical conditions that prevailed during uranium transport and further trapping in opal. Analyses of one thick-section and Focused Ion Beam (FIB) ultrathin sections of one opal sample, using Scanning Electron Microscopy (SEM), Transmission Electron Microscopy (TEM), Selected Area Electron Diffraction (SAED), and Energy Dispersive X-ray Spectrometry (EDXS). These techniques provided evidence for the presence of vorlanite nanoscale crystals. They are found within U-rich, but amorphous, opal zones retaining a Ca:U ratio of 1:1, which could have played the role of precursor for vorlanite crystallization.

MATERIAL AND METHODS

Samples

Opals at Nopal I fill fractures, pores and cavities in the subsurface (Cesbron et al. 1993; Calas et al. 2008; Schindler et al. 2010). They belong to the A (amorphous)-type, as shown by X-ray diffraction (XRD) analyses (Schindler et al. 2010). Opals at Nopal I can overlie kaolinite, hematite and uranyl minerals and display green or yellow colors. A detailed paragenesis of the uranium-bearing minerals at the Nopal I deposit has been described recently (Fayek et al. 2006; Calas et al. 2008; Angiboust et al. 2012). The sample used in this study consists of yellow opal and comes from an exposed surface of the Nopal I uranium deposit. One thick-section of this sample was prepared to examine the macro- and micro-

layering in the sample. Two FIB ultrathin sections were prepared from this thick-section for TEM analysis.

Scanning electron microscopy (SEM) and electron probe micro-analysis (EPMA)

Scanning electron microscopy (SEM) images were obtained using a Zeiss Ultra 55 SEM-FEG UHR (IMPMC, Paris). Semi-quantitative analyses were performed using a Brucker Quantax energy-dispersive X-ray spectrometer (EDXS). Quantitative analyses were collected using a Cameca SX-100 electron microprobe. Operating conditions were 15 kV accelerating voltage, 20 nA beam current, and data acquisition in wavelength-dispersive spectrometry (WDS) mode.

Focused ion beam (FIB) milling

A focused ion beam (FIB) was used to prepare electron transparent samples for transmission electron microscopy (TEM) analysis. FIB milling was performed with a Zeiss CrossBeam Neon40 EsB workstation (IMPMC, Paris). A description of the FIB preparation of TEM samples can be found in Heaney et al. (2001).

Transmission electron microscopy (TEM)

TEM analysis were carried out on a JEOL 2100F microscope (IMPMC, Paris) operating at 200 kV, equipped with a field emission gun, a high-resolution (UHR) pole piece and a Gatan energy filter GIF 2001. Scanning transmission electron microscopy (STEM) in high angle annular dark field (HAADF) allowed Z-contrast imaging. Qualitative elemental compositions were determined by EDXS performed using a JEOL detector with an ultrathin window allowing detection of light elements. Selected area electron diffraction (SAED) patterns were obtained with a Gatan US 4000 CCD camera. Taking into account the specific

signature of carbonate at the C-K edge (Benzerara et al. 2006), qualitative measurements of the carbonate content were carried out by electron energy-loss spectroscopy (EELS) using a Gatan GIF 2001 system. Since the observed crystalline phases readily amorphize under electron beam irradiation, we used low-intensity beam conditions to minimize the electron dose and subsequent beam damage.

RESULTS

The mineralogy of opal-filled fractures in the rhyolitic tuff was investigated at the microscopic scale using SEM and EPMA. The yellow opal sample from an exposed surface of the Nopal I uranium deposit shows two successive infillings of the fissure with uranyl silicates overlain by opal in accordance with Schindler et al. (2010). Uranium occurs under various forms within the opal. The SEM picture in Figure 1 shows the occurrence of micrometer-size particles of uranophane embedded in opal similar to the ß-uranophane crystals coated by late opal described by Cesbron et al. (1993). Electron microprobe and TEM-EDXS analyses also indicate the presence of ß-uranophane $Ca[(UO_2)(SiO_3OH)]_2(H_2O)_5$, apatite $Ca_5(PO_4)_3(HO, F)$ and kaolinite $Al_2Si_2O_5(OH)_4$ with minor amounts of iron oxides in the vicinity (Fig. 1 and supporting information: Fig. S1). Details on the morphology and chemical composition of these phases are given in the Supporting Information.

Opal exhibits concentric features with a zoning reflected in variations of uranium concentration (Fig. 1). In all patterns, the concentrations of Ca and U are positively correlated, retaining a Ca:U atomic ratio of 1:1. The average concentration measured by electron microprobe for Ca and U is 0.24 and 1.41 wt. %, respectively (Supporting information, Table S1). These results are consistent with recent studies (Schindler et al. 2010).

The Ca-U zone is quite homogeneous (cf., supporting information: Fig. S2a) and no carbonates were detected by TEM-EELS. Nanophases were identified with TEM in the bright field mode (Fig. 2a). Their SAED patterns (Figs. 3a, 3b and 3c) indicate a *Fm*-3*m* structure and TEM-EDXS shows the presence of Ca and U (Fig. 2b). The particles show the following d_{hkl}-spacings: d_{111} = 3.13 Å; d_{200} = 2.70 Å; d_{133} = 1.24 Å; d_{024} = 1.21 Å and d_{242} = 1.11 Å. These values yield a refined unit-cell parameter a = 5.42(5) Å and a unit-cell volume V = 159.2(44) Å^3 using UnitCell (Holland and Redfern 1997). These d_{hkl} spacings match those of vorlanite (CaU^{6+})O_4 (*Fm*-3*m*, a = 5.3813(2) Å, V = 155.834(10) Å^3, Galuskin et al. 2011) determined from single-crystal XRD: d_{111} = 3.105 Å; d_{200} = 2.690 Å; d_{133} = 1.235 Å; d_{024} = 1.203 Å and d_{242} = 1.099 Å. Our d_{hkl} values are a little higher than those found by Galuskin et al. (2011). Such a discrepancy could be due to the error inherent in determining d-spacings from SAED patterns. The presence of vorlanite can also be shown by the matching between SAED patterns of the nanocrystals and SAED patterns simulated using the structure of vorlanite (Figs. 3a, 3b and 3c). Figure 3d shows the cubic oxygen coordination of U^{6+} in this mineral. All vorlanite nanocrystals observed correspond to euhedral cubes, 20 to 150 nm large (Fig. 2a and inset in Fig. 3a). After a careful SAED analysis performed onto the whole ultrathin section using low-beam intensity conditions, we checked by high-resolution TEM (HRTEM) that in most parts of the sample examined only amorphous phases (opal A, i.e. amorphous silica) were present. These phases devoid of non-beam-sensitive nanocrystals were found to contain minor amounts of Ca and U using EDXS (supporting information: Fig. S2).

DISCUSSION

Among the oxidized uranium-bearing minerals, most U(VI) species occur as uranyl $(UO_2)^{2+}$ species, while few uranate minerals with U^{6+} are known (Finch and Murakami 1999). For instance, only one high temperature uranate mineral is known, clarkeite, $Na[(UO_2)O(OH)]$, suggested to form above 200°C (Finch and Ewing 1997). It is isostructural with the rhombohedral form of $CaUO_4$, which has not yet been found in nature. Besides, the cubic form of $CaUO_4$, vorlanite, has been recently described in Upper Chegem caldera, Northern Caucasus, Russia (Galuskin et al. 2011). Vorlanite has a fluorite-type structure, being isostructural with uraninite. U^{6+} cations are 8-coordinated by equidistant O atoms (Fig. 3d), at variance with the geometry of linear UO_2^{2+} uranyl ions. The cubic morphology of the nanocrystals of vorlanite in the Nopal U-deposit is in agreement with its crystal structure. By contrast, there was a discrepancy between the rhombohedral shape of vorlanite crystals from the Upper Chegem caldera and its cubic structure: it has been suggested that these vorlanite crystals resulted from the further transformation of the high-temperature rhombohedral polymorph of $CaUO_4$ ("protovorlanite") to the cubic polymorph, vorlanite, under irradiation arising from U-decay (Galuskin et al. 2011, 2012). The formation conditions of vorlanite in its two known occurrences are then different and shed light on the genetic significance of vorlanite.

Our data show the same Ca/U = 1 ratio for vorlanite and U-rich opal, which indicates an early trapping of vorlanite components. Nopal I opals formed at around 30°C (Calas et al. 2008; Schindler et al. 2010). Thus, vorlanite may have formed at low temperature during opal maturation in zones locally supersaturated in Ca and U, which may have played the role of precursor by retaining a Ca/U ratio of 1. Other minerals form on SiO_2 surfaces, e.g., hydroxyapatite on porous sol-gel-derived SiO_2 substrates (e.g., Peltola et al. 1999). Although the U content of the solution was below the solubility of uranophane according to experimental data (Langmuir 1978; Zielinski 1980), the solubility of vorlanite under these

conditions remains unknown.

The nano-size of vorlanite crystals in opals from Nopal I is novel. It may influence the formation and stability conditions of vorlanite, as it is known that phase stability may differ significantly with particle size decreasing down to the nm range (Banfield and Zhang 2001). To our knowledge, no cubic calcium uranate $CaUO_4$ has been synthesized and there are no thermodynamic constraints on its formation and stability conditions. However, a few experimental studies provide pH values consistent with the formation of uranates. Ritherdon et al. (2003) studied the U(VI)-Ca^{2+}-SiO_2-OH system and observed the occurrence of a rhombohedral calcium uranate above pH 8. Additional data are needed to constrain the conditions of formation of vorlanite. The difficulty of determining the presence of nanosized vorlanite, due to its instability under the electron beam, may result in missing this mineral in oxidized low temperature U-parageneses, despite the fact that uranates may play a more important role than expected in the U behaviour in low-temperature environments.

AKNOWLEDGEMENTS

We thank O. Boudouma and F. Couffignal from the Service MEB, Université Pierre et Marie Curie. We also thank L. Galoisy from the IMPMC for sampling the investigated opal sample during the Nopal field trip on December 2006. This research was partially funded by a NSERC discovery grant to Fayek and the CRC program.

REFERENCES

Allard, T., Ildefonse, P., Beaucaire, C. and Calas, G. (1999) Structural chemistry of uranium associated with Si, Al, Fe gels in a granitic uranium mine. Chemical Geology, 158, 81-103.

Angiboust, S., Fayek, M., Power, I., Camacho, A., Calas, G. and Southam, G. (2012) Structural and biological control of the Cenozoic epithermal uranium concentrations from the Sierra Peña Blanca, Mexico. Mineralium Deposita, in press. DOI: 10.1007/s00126-012-0408-5.

Banfield, J.F. and Zhang, H. (2001) Nanoparticles and the Environment. In J.F. Banfield, and A. Navrotsky, Eds., Nanoparticles in the environment, 44, p. 1-58. Reviews in Mineralogy and Geochemistry, Mineralogical Society of America, Washington, DC.

Benzerara, K., Menguy, N., López-García, P., Yoon, T.-H., Kazmierczak, J., Tyliszczak, T., Guyot, F. and Brown Jr., G.E. (2006) Nanoscale detection of organic signatures in carbonate microbialites. Proceedings of the National Academy of Sciences, 103, 9440-9445.

Calas, G., Agrinier, P., Allard, T. and Ildefonse, P. (2008) Alteration geochemistry of the Nopal I uranium deposit (Sierra Peña Blanca, Mexico), a natural analogue for a radioactive waste repository in volcanic tuffs. Terra Nova, 20, 206-212.

Cesbron, F., Ildefonse, P. and Sichere, M.C. (1993) New mineralogical data on uranophane and β-uranophane: synthesis of uranophane. Mineralogical Magazine, 57, 301-308.

Duff, M.C., Coughlin, J.U. and Hunter, D.B. (2002) Uranium co-precipitation with iron oxide minerals. Geochimica et Cosmochimica Acta, 66, 3533-3547.

Fayek, M., Ren, M., Goodell, P., Dobson, P., Saucedo, A.L., Kelts, A., Utsunomiya, S., Ewing, R.C., Riciputi, L.R. and Reyes, I. (2006) Paragenesis and geochronology of the Nopal I uranium deposit, Mexico. D.T. Goddard, Ed., Proceedings of the Eleventh International High-Level Radioactive Waste Management Conference, Las Vegas, NV, p. 55-62. American Nuclear Society, La Grange Park, IL.

Finch, R.J. and Ewing, R.C. (1997) Clarkeite; new chemical and structural data. American

Mineralogist, 82, 607-619.

Finch, R.J. and Murakami, T. (1999) Systematics and paragenesis of uranium minerals. In P.C. Burns, and R. Finch, Eds., Uranium: Mineralogy, Geochemistry and the Environment, 38, p. 91-179. Reviews in Mineralogy, Mineralogical society of America, Washington, D.C.

Galuskin, E.V., Armbruster, T., Galuskina, I.O., Lazic, B., Winiarski, A., Gazeev, V.M., Dzierzanowski, P., Zadov, A.E., Pertsev, N.N., Wrzalik, R., Gurbanov, A.G. and Janeczek, J. (2011) Vorlanite (CaU6+)O4 - A new mineral from the Upper Chegem caldera, Kabardino-Balkaria, Northern Caucasus, Russia. American Mineralogist, 96, 188-196.

Galuskin, E.V., Galuskina, I.O., Dubrovinsky, L.S. and Janeczek, J. (2012) Thermally induced transformation of vorlanite to "protovorlanite": Restoration of cation ordering in self-irradiated CaUO4. American Mineralogist, 97, 1002-1004.

Heaney, P.J., Vicenzi, E.P., Giannuzzi, L.A. and Livi, K.J.T. (2001) Focused ion beam milling: A method of site-specific sample extraction for microanalysis of Earth and planetary materials. American Mineralogist, 86, 1094-1099.

Holland, T.J.B. and Redfern, S.A.T. (1997) Unit cell refinement from powder diffraction data; the use of regression diagnostics. Mineralogical Magazine, 61, 65-77.

Langmuir, D. (1978) Uranium solution-mineral equilibria at low temperatures with applications to sedimentary ore deposits. Geochimica et Cosmochimica Acta, 42, 547-569.

Novikov, A.P., Kalmykov, S.N., Utsunomiya, S., Ewing, R.C., Horreard, F., Merkulov, A., Clark, S.B., Tkachev, V.V. and Myasoedov, B.F. (2006) Colloid Transport of Plutonium in the Far-Field of the Mayak Production Association, Russia. Science, 314, 638-641.

Peltola, T., Jokinen, M., Rahiala, H., Levänen, E., Rosenholm, J.B., Kangasniemi, I. and Yli-Urpo, A. (1999) Calcium phosphate formation on porous sol-gel-derived SiO2 and CaO-P2O5-SiO2 substrates in vitro. Journal of Biomedical Materials Research, 44, 12-21.

Ragnarsdottir, K.V. and Charlet, L. (2000) Uranium behaviour in natural environment. In J.D. Cotter-

Howells, L.S. Campbell, E. Valsami-Jones, and M. Batchelder, Eds., Environmental Mineralogy: Microbial Interactions, Anthropogenic Influences, Contaminated Lands And Waste Management, Mineralogical Society Series 9, p. 245-289Mineralogical Society of Great Britain & Ireland, London.

Ritherdon, B., Phelps, C., Neff, H., Sowder, A.G. and Clark, S.B. (2003) Stability of U(VI) solid phases in the U(VI)-Ca^{2+}-SiO_2-OH system. Radiochimica Acta, 91, 93-96.

Schindler, M., Fayek, M. and Hawthorne, F.C. (2010) Uranium-rich opal from the Nopal I uranium deposit, Peña Blanca, Mexico: evidence for the uptake and retardation of radionuclides. Geochimica et Cosmochimica Acta, 74, 187-202.

Zielinski, R.A. (1980) Uranium in secondary silica: a possible exploration guide. Economic Geology, 75, 592-602.

253 **FIGURE CAPTIONS**

254

255 **Figure 1.** BSE SEM photo of the yellow opal sample from an exposed surface of the Nopal I
256 uranium deposit. The uraniferous opal is characterized by an atomic Ca:U ratio = 1:1 and an
257 uranium concentration from 0.1 to 4 wt%. In the opal, the clear patterns are U-rich regions.
258 Dotted white lines show FIB milling areas used to prepare TEM samples.

259 **Figure 2.** (a) TEM picture in the bright field mode of the Ca-U zone thin cross-section
260 showing various-sized vorlanite nanoparticles and (b) EDXS spectrum in this zone (the
261 intense Si and O contributions come from the surrounding opal).

262 **Figure 3.** (a to c) SAED patterns of vorlanite particles with different zone axis (calculated
263 vorlanite diffraction pattern is given in green). TEM picture in the bright field mode of one
264 vorlanite particle corresponding to the (a) SAED pattern and showing its cubic morphology is
265 given in (a) inset. (d) Model showing the cubic oxygen coordination of U^{6+} in vorlanite
266 $CaUO_4$ (after Galuskin et al. 2011).

This is a preprint, the final version is subject to change, of the American Mineralogist (MSA)
Cite as Authors (Year) Title. American Mineralogist, in press.
(DOI will not work until issue is live.) DOI: http://dx.doi.org/10.2138/am.2013.4295

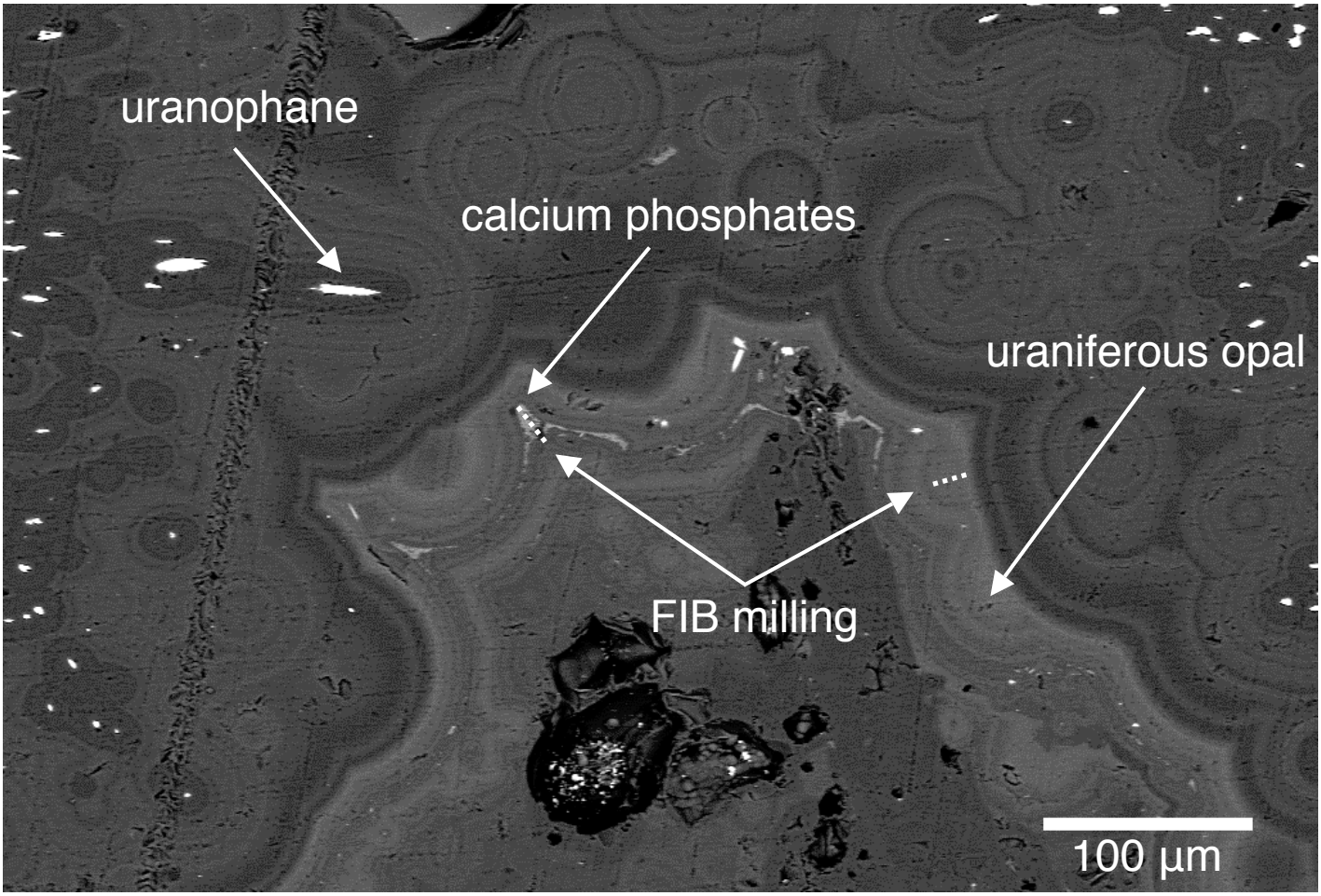

Figure 1

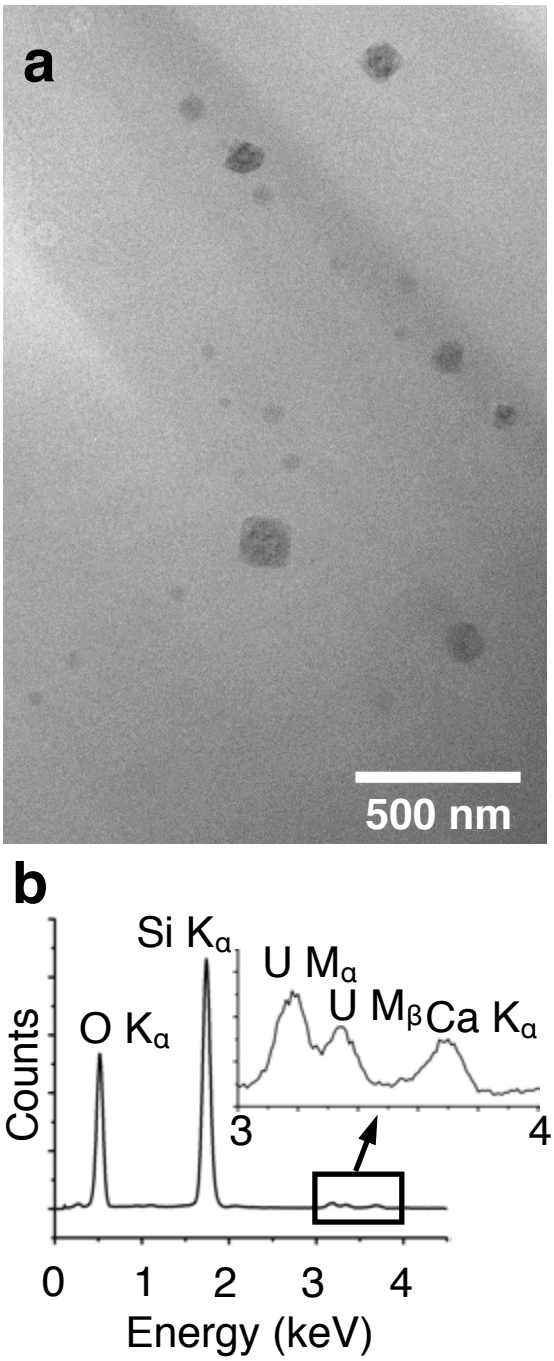

Figure 2

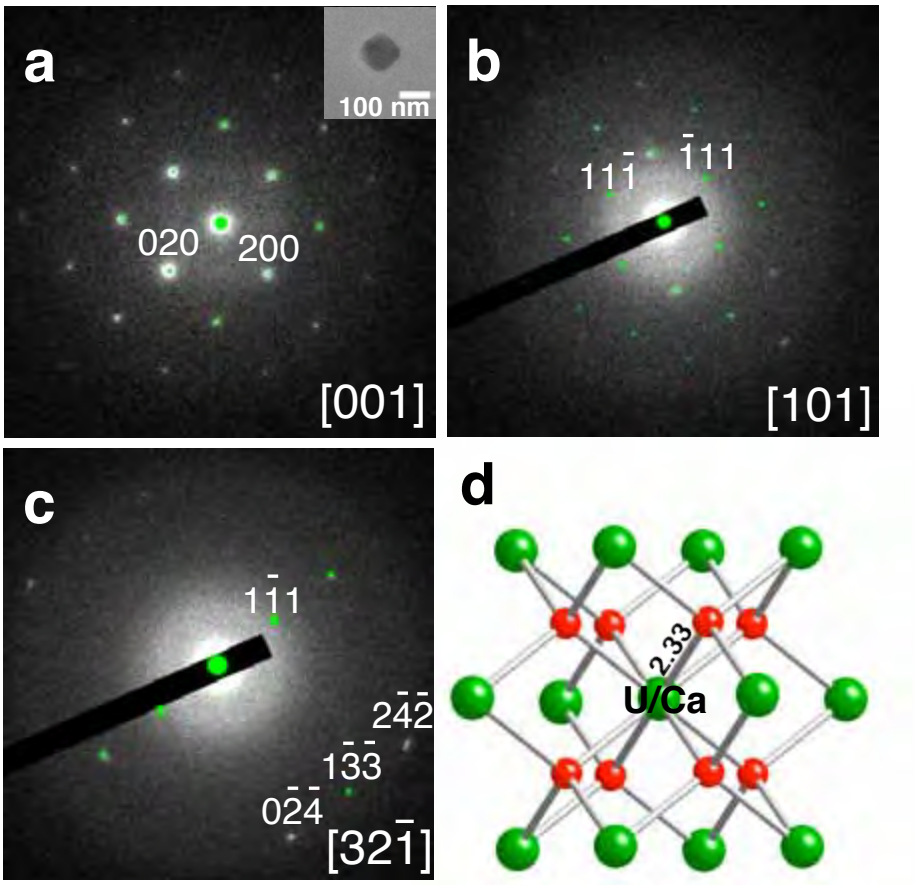
a
100 nm
020
200
[001]
b
$1\bar{1}1$
$\bar{1}11$
[101]
c
$\bar{1}11$
$2\bar{4}\bar{2}$
$1\bar{3}\bar{3}$
$0\bar{2}\bar{4}$
$[32\bar{1}]$
d
2.33
U/Ca

Figure 3